



Suramlishvili, N., Eggers, J. G., Hoppe, J., & Hynek, M. (2015). Singularities of relativistic membranes. *Geometric Flows*, 1(1), 17-33. 10.1515/geofl-2015-0003

Publisher's PDF, also known as Final Published Version

Link to published version (if available):
[10.1515/geofl-2015-0003](https://doi.org/10.1515/geofl-2015-0003)

[Link to publication record in Explore Bristol Research](#)
PDF-document

University of Bristol - Explore Bristol Research

General rights

This document is made available in accordance with publisher policies. Please cite only the published version using the reference above. Full terms of use are available:
<http://www.bristol.ac.uk/pure/about/ebr-terms.html>

Take down policy

Explore Bristol Research is a digital archive and the intention is that deposited content should not be removed. However, if you believe that this version of the work breaches copyright law please contact open-access@bristol.ac.uk and include the following information in your message:

- Your contact details
- Bibliographic details for the item, including a URL
- An outline of the nature of the complaint

On receipt of your message the Open Access Team will immediately investigate your claim, make an initial judgement of the validity of the claim and, where appropriate, withdraw the item in question from public view.

Research Article

Open Access

J. Eggers, J. Hoppe*, M. Hynes, and N. Suramlishvili

Singularities of relativistic membranes

Abstract: Pointing out a crucial relation with caustics of the eikonal equation we discuss the singularity formation of 2-dimensional surfaces that sweep out 3-manifolds of zero mean curvature in $\mathbb{R}^{3,1}$.

DOI 10.1515/geofl-2015-0003

Received February 2, 2015; accepted February 23, 2015

1 Introduction

While interest in the singularity formation of cosmic strings goes back more than three decades [10] and the fact that any closed curve sweeping out a zero-mean-curvature surface in $\mathbb{R}^{2,1}$ necessarily becomes singular in finite time was noted already 20 years ago ([5], including examples of singularity-propagations preventing collaps to a point), a full mathematical treatment, including the above mentioned phenomena, appeared only recently [8].

Here we continue our investigation of M-brane singularity formation ([4], [2]) and for the first time attack the case of (not necessarily axially symmetric) membrane motions, with methods that in principle can be used for even higher dimensional extended objects.

Because of an intimate relation with the eikonal equation, we first describe the singularity formation for 2-dimensional surfaces moving normally with unit speed. Then we discuss a corresponding Ansatz for the second order Born-Infeld equation (which describes the time-evolution of the graph of a relativistic membrane) and provide numerical data, resp. pictures, showing the singularity formation in some examples.

2 Relativistic M-branes

Let us consider the motion of an M-dimensional extended object in Minkowski space $\mathbb{R}^{M+1,1}$ sweeping out an $M + 1$ dimensional manifold parametrized by $u = (u^0, \mathbf{u})$, cp [6]. Stationary points of the world volume

$$S = \int du^{M+1} \sqrt{G} \quad (1)$$

correspond to solutions of

$$\frac{1}{\sqrt{G}} \partial_\alpha (\sqrt{G} G^{\alpha\beta} \partial_\beta x^\mu) = 0, \quad \mu = 0, \dots, M + 1, \quad (2)$$


G and $G_{\alpha\beta}$, $\alpha, \beta = 0, \dots, M$, being the (absolute value of) the determinant respectively the inverse of the induced metric $G_{\alpha\beta} := \frac{\partial x^\mu}{\partial u^\alpha} \frac{\partial x^\nu}{\partial u^\beta} \eta_{\mu\nu}$, $\eta_{\mu\nu} = \text{diag}(1, -1, \dots, -1)$. Choosing $u^0 = x^0 =: t$ and $\dot{\mathbf{x}} \partial_a \mathbf{x} = 0$, $a = 1, \dots, M$, so that \mathbf{x} in $(x^\mu) = (t, \mathbf{x}(t, u^1, \dots, u^M))$ describes a time-dependent surface moving orthogonal to itself in \mathbb{R}^{M+1} , the $\mu = 0$ component of (2) takes the form of a local conservation law

$$\partial_t \sqrt{\frac{g}{1 - \dot{\mathbf{x}}^2}} = 0 \quad (3)$$

***Corresponding Author: J. Hoppe:** Department of Mathematics, Royal Institute of Technology, 100 44 Stockholm, Sweden, KIAS and Sogang University, 121-742 Seoul, Korea, E-mail:hoppe@itp.phys.ethz.ch

J. Eggers, N. Suramlishvili: School of Mathematics, University of Bristol, University Walk, Bristol BS8 1TW, United Kingdom

M. Hynes: Department of Mathematics, Royal Institute of Technology, 100 44 Stockholm, Sweden

 © 2015 J. Eggers et al., licensee De Gruyter Open.

This work is licensed under the Creative Commons Attribution-NonCommercial-NoDerivs 3.0 License.

so that the first order system

$$\begin{aligned}\dot{\mathbf{x}}^2 + \frac{g}{\rho^2} &= 1 \\ \dot{\mathbf{x}} \partial_a \mathbf{x} &= 0\end{aligned}\tag{4}$$

is implied ($\rho(\mathbf{u}) := \sqrt{\frac{g}{1-\dot{\mathbf{x}}^2}}$, and g being the determinant of the metric $g_{rs} := \partial_r \mathbf{x} \cdot \partial_s \mathbf{x}$, $r, s = 1, \dots, M$, induced on the hypersurface), and for co-dimension one the $\mu = i = 1, \dots, M + 1$ part of (2) follows from (4) as long as the velocity $\dot{\mathbf{x}}$ and the tangent vectors $\partial_a \mathbf{x} = \frac{\partial}{\partial u^a} \mathbf{x}$ are linearly independent (cp. [5]).

In this note we explore (4), both analytically and numerically, for various cases, focusing on singularity formation. The key observation in our analysis is the fact (cp.(3), which gives a 1-1 correspondence between $|\dot{\mathbf{x}}| \rightarrow 1$ and $\sqrt{g} \rightarrow 0$, i.e. the hypersurface developing a singularity) that solutions of (4) around a singular point are close to those of

$$\begin{aligned}\dot{\mathbf{x}}^2 &= 1 \\ \dot{\mathbf{x}} \partial_a \mathbf{x} &= 0, \quad a = 1, \dots, M\end{aligned}\tag{5}$$

which (assuming that the points of the hypersurface either all move inwards or all move outwards) is equivalent to the eikonal equation

$$\dot{\mathbf{x}} = \mathbf{n}.\tag{7}$$

In chapter 2 we consider the eikonal equation in detail, providing a description of its singular solutions, in chapter 3 derive a second order shape-equation for membranes, in chapter 4 discuss axially symmetric membranes and in chapter 5 we present some numerical solutions to the evolution equations (4) for $M=2$.

3 The eikonal equation

For hypersurfaces locally described as graphs, an equivalent formulation of (7) is

$$\mathcal{L}^2 = 1 - \dot{z}^2 + \nabla z^2 = 0.\tag{8}$$

This can be seen as follows. Let $\mathbf{x} = (\mathbf{x}_{\parallel}, z)$, so that $z = h(\mathbf{x}_{\parallel}, t)$ satisfies (8)

$$\frac{\partial h}{\partial t} = \sqrt{1 + \nabla_{\parallel} h^2}.\tag{9}$$

Define $C(\mathbf{x}, t) = h(\mathbf{x}_{\parallel}, t) - z$, so that $C(\mathbf{x}(\mathbf{u}, t), t) = 0$. It follows that

$$0 = \frac{dC(\mathbf{x}(\mathbf{u}, t), t)}{dt} = \frac{\partial C}{\partial t} + \dot{\mathbf{x}}(\mathbf{u}, t) \cdot \nabla C = \frac{\partial h}{\partial t} + \dot{\mathbf{x}} \cdot (\nabla_{\parallel} h, -1).$$

But

$$\mathbf{n} = \frac{(-\nabla_{\parallel} h, 1)}{\sqrt{1 + \nabla_{\parallel} h^2}},$$

and so

$$\dot{\mathbf{x}} \cdot \mathbf{n} = 1.\tag{10}$$

Note that (in arbitrary dimensions) solutions of (8) automatically solve the membrane equation for a surface written as a graph:

$$(1 - z_{\alpha} z^{\alpha}) \square z + z^{\beta} z^{\alpha} z_{\alpha\beta} = 0.\tag{11}$$

While this does not immediately imply that all singularities of (11) are described by the eikonal equation, it can be shown for co-dimension 1 surfaces using the following argument: consider the parametric form of a

hypersurface, $\mathbf{x}(\mathbf{u}, t)$, for example in three dimensions: $\mathbf{x}(\varphi^1, \varphi^2, t)$. Then the dynamical equation (4) can be written as

$$\dot{\mathbf{x}} = \pm \sqrt{1 - g/\rho^2} \mathbf{n}, \quad (12)$$

where \mathbf{n} is the normal to the surface. The value of ρ is determined by the initial condition. Once ρ is known, (12) can be solved as a first-order equation, and one expects that its solutions (as functions of the parameters \mathbf{u} , resp. (φ^1, φ^2)) remain smooth for all times (confirmed by the numerical results). This means that the only singularities come from the fact that the tangent vectors become linearly dependent, resp. $\sqrt{g} = |\partial_1 \mathbf{x} \times \partial_2 \mathbf{x}|$ going to 0. This means that near the singular time $v \equiv \sqrt{1 - g/\rho^2} \approx 1$, i.e. solutions are close to those of the eikonal equation.

3.1 Solutions of the eikonal equation

Solutions of the eikonal equation are wavefronts propagating in space with unit speed. According to Huygens' principle, (8) is equivalent to saying that from each point of a wavefront emanates a ray which moves at constant speed 1 in the normal direction. To construct the wavefront at future times t , one simply has to connect the points to which each individual ray has progressed. Writing a surface in $M + 1$ dimensions as $\mathbf{x}(\mathbf{u}, t)$, where \mathbf{u} is an M -dimensional vector parameterizing the surface, and thus parameterizing rays, Huygens solution says

$$\mathbf{x}(\mathbf{u}, t) = \mathbf{x}(\mathbf{u}, 0) + \mathbf{n}(\mathbf{u}, 0)t, \quad (13)$$

where $\mathbf{n}(\mathbf{u}, 0)$ is the normal to the initial wave front. To show that (13) satisfies (7), it remains to note that $\mathbf{n}(\mathbf{u}, t) = \mathbf{n}(\mathbf{u}, 0)$ for all t : differentiating (13) with respect to any component u of \mathbf{u} , we obtain a tangent vector to the surface

$$\partial_a \mathbf{x}(\mathbf{u}, t) = \partial_a \mathbf{x}(\mathbf{u}, 0) + \partial_a \mathbf{n}(\mathbf{u}, 0)t.$$

Multiplying by $\mathbf{n}(\mathbf{u}, 0)$, we have

$$\mathbf{n}(\mathbf{u}, 0) \cdot \partial_a \mathbf{x}(\mathbf{u}, t) = \mathbf{n}(\mathbf{u}, 0) \cdot \partial_a \mathbf{n}(\mathbf{u}, 0)t = 0.$$

Let $z(\mathbf{u}, 0) = f(\mathbf{u})$ be the graph representation of the initial wave front (in any dimension), so $\mathbf{x}(\mathbf{u}, 0) = (\mathbf{u}, f(\mathbf{u}))$. Then

$$\mathbf{n}(\mathbf{u}, 0) = \frac{(-\nabla f, 1)}{\sqrt{1 + \nabla f^2}},$$

and (13) yields

$$\mathbf{x}(\mathbf{u}, t) = \mathbf{x}(\mathbf{u}, 0) + \frac{(-\nabla f, 1)}{\sqrt{1 + \nabla f^2}} t.$$

In other words, the solution is

$$\mathbf{x}_{\parallel} = \mathbf{u} - \frac{\nabla f}{\sqrt{1 + \nabla f^2}} t, \quad (14)$$

$$z = f(\mathbf{u}) + \frac{t}{\sqrt{1 + \nabla f^2}}. \quad (15)$$

For a smooth initial condition $\mathbf{x}(\mathbf{u}, 0)$, each component of (13) is a smooth function for all t . Singularities in the shape of the wave front only arise if the mapping $\mathbf{u} \mapsto \mathbf{x}$ no longer has full rank, which is precisely the situation described by singularity theory [1]

3.2 Solutions around a singularity

Singularities of wave fronts of (8) are described by catastrophe theory in [1, 7], where they are classified according to their codimension, i.e. the number of parameters one needs to adjust in order to lie on a singularity.

The simplest catastrophe is the fold, with codimension one [7], which means that the singularities of a wave front (the caustics) generically lie on a two-dimensional surface in three-dimensional space. Using time as an additional parameter, the point where a singularity occurs *first* is described by the cusp catastrophe, which has codimension two. Near this singularity, the caustic surface has the shape of a cusp (see below), hence the name. Catastrophes of higher order are also possible, but they would require to tune the initial condition to a particular form, and are thus non-generic.

To find the spatial structure of the generic singularity, we start from the solution (14),(15), and expand about the singularity. Taking $\mathbf{u} = (\varphi, \psi)$, the generic form of the initial wave is

$$f = \varphi^2 + b\psi^2 + a_3\psi^3 + b_3\varphi\psi^2 + a_4\psi^4 + b_4\varphi\psi^3 + c_4\varphi^2\psi^2 + d_4\varphi^3\psi + e_4\varphi^4. \quad (16)$$

Terms linear in φ and ψ can be eliminated by a shift of the coordinate system, and the mixed term $\varphi\psi$ by a rotation. Higher order terms are neglected, because they only lead to subleading contributions to the singular wavefront. We have chosen the length scale to normalize the curvature of the wave front in the x -direction to 2, which means a singularity first occurs at $t_0 = 1/2$. For this to be consistent, we must have $b < 1$. There is no term φ^3 or $\varphi^2\psi$, because each of them would lead to a higher curvature for $\varphi \neq 0$ or $\psi \neq 0$ respectively, and thus to a singularity for time $t < t_0$.

We insert (16) into (14),(15), and expand the solution in $t' = t_0 - t$, with $\varphi \sim \psi \sim t'^{1/2}$. We expand x and y to order $t'^{3/2}$ and z to order t'^2 , where y has the structure

$$y = (1 - b)\psi + (\dots)\psi^2 + \dots + \varphi^2\psi + \dots$$

Solving this equation perturbatively for ψ in terms of y and φ , in order to eliminate ψ , one gets (using MAPLE):

$$x = By^2 + 2t'\varphi + 2A_1\varphi^3 + 2A_2\varphi y^2 + \frac{3A_3}{2}\varphi^2 y + A_4 y^3, \quad (17)$$

$$z = t_0 - t' + Ay^2 + Cy^3 + 2t'\varphi^2 + 3A_1\varphi^4 + 2A_2\varphi^2 y^2 + 2A_3\varphi^3 y + A_5 y^4 - 2A^2 t' y^2, \quad (18)$$

where

$$\begin{aligned} B &= -\frac{b}{2(1-b)^2}, \quad A_1 = 1 - e_4, \quad A_2 = -\frac{b_3^2}{2(1-b)^3} + \frac{b^2}{(1-b)^2} - \frac{c_4}{2(1-b)^2}, \\ A_3 &= -\frac{d_4}{1-b}, \quad A_4 = -\frac{b_4}{2(1-b)^3} - \frac{3a_3 b_3}{2(1-b)^4}, \\ A_5 &= -\frac{4a_4 - 4b^4 - b_3^2}{4(1-b)^4} + \frac{9a_3^2}{4(1-b)^5}, \quad A = \frac{b}{1-b}, \quad C = \frac{a_3}{(1-b)^3}. \end{aligned} \quad (19)$$

Cast in similarity form:

$$X = \frac{x - By^2}{|t'|^{3/2}} = \pm 2\zeta + 2A_1\zeta^3 + 2A_2\zeta Y^2 + \frac{3A_3}{2}\zeta^2 Y + A_4 Y^3, \quad (20)$$

$$h = \frac{z - t_0 + t' - Ay^2 - Cy^3}{|t'|^2} = \pm 2\zeta^2 + 3A_1\zeta^4 + 2A_2\zeta^2 Y^2 + 2A_3\zeta^3 Y + A_5 Y^4 \mp 2A^2 Y^2, \quad (21)$$

where $\zeta = \varphi/|t'|^{1/2}$, and $Y = y/|t'|^{1/2}$, via the \pm signs making sure that the description works both for $t' > 0$ (before the singularity) and $t' < 0$ (after the singularity).

We now calculate the places where for $t' < 0$ singularities appear on the wave front, which in optics are known as caustics [7] (places of high light intensity). They are determined by $g = 0$ or (equivalently, since $g = D_1^2 + D_2^2 + D_3^2$) the condition that the rank of

$$D = \begin{pmatrix} x_\varphi & y_\varphi & z_\varphi \\ x_\psi & y_\psi & z_\psi \end{pmatrix} \quad (22)$$

is not maximal, where by D_1, D_2, D_3 we denote the minors of D . Using the fact that $\ell(\mathbf{x}(\varphi, \psi)) = t$, where ℓ is the Euclidean distance between $\mathbf{x}(\mathbf{u}, t)$ and $\mathbf{x}(\mathbf{u}, 0)$, and the ray conditions [7] $\ell_\varphi = \ell_\psi = 0$, one can show that

$$D_1 = \begin{vmatrix} x_\varphi & y_\varphi \\ x_\psi & y_\psi \end{vmatrix} = 0 \quad (23)$$

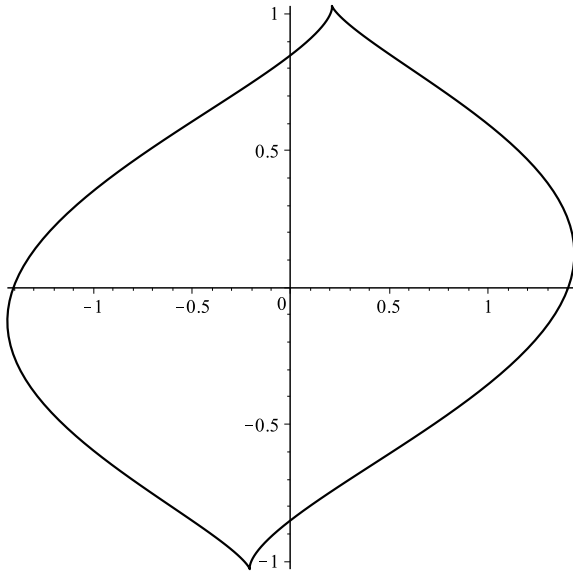


Figure 1: A typical image of the places where the wave front has a singularity, projected onto the $x - y$ plane, as described by (25) and (27). The width of this “lip” shape scales like $|t'|^{3/2}$, the height like $|t'|^{1/2}$.

is a necessary and sufficient (!) condition for a singularity to occur. Expanding D_1 to second order, this yields

$$-t' = A_2 y^2 + \frac{3A_3}{2} \varphi y + 3A_1 \varphi^2, \quad (24)$$

the similarity form of which is

$$1 = A_2 Y^2 + \frac{3A_3}{2} \zeta Y + 3A_1 \zeta^2. \quad (25)$$

Inserting (24) into (17) yields the caustic surface

$$x - By^2 = -4A_1 \varphi^3 - \frac{3A_3}{2} \varphi^2 y + A_4 y^3, \quad z - t_0 = 3A_1 \varphi^2 + \frac{3A_3}{2} \varphi y + (A + A_2) y^2, \quad (26)$$

with similarity form

$$X = -4A_1 \zeta^3 - \frac{3A_3}{2} \zeta^2 Y + A_4 Y^3, \quad Z = \frac{z - t_0}{|t'|} = 3A_1 \zeta^2 + \frac{3A_3}{2} \zeta Y + (A + A_2) Y^2. \quad (27)$$

Notice that for $A_2 = A_3 = A_4 = A = 0$ this is a cusp, but even the deformed caustic surface with generic values of A_2, A_3, A_4 , and A is equivalent to the y -independent cusp up to smooth transformations [7]. The shape of cuts through the wavefront itself is that of a swallowtail [4], as will be illustrated by our simulations below.

To get an idea of how the singularities on a wave front lie in space (which will be lines in three-dimensional space), one has to consider (24) at a fixed time $t' < 0$. Projected onto the plane $Z = 0$, the similarity description of this is described by (25) and the first equation of (27). A typical curve is plotted in Fig. 1, which has a “lip” shape, known from optics [7] and wave breaking [9].

3.3 Similarity equation

The singular solution (20), (21) can also be obtained considering similarity solutions of the eikonal equation (8). This approach has the advantage of being generalizable to problems for which exact solutions are not available [3], such as the membrane equation (11). We make the ansatz suggested by (20) and (21),

$$z = \mp |t'| g_1(Y) + |t'|^{3/2} g_2(Y) + |t'|^2 h(X, Y), \quad X = \frac{x - By^2}{|t'|^{3/2}}. \quad (28)$$

Then

$$\dot{z} = g_1 - \frac{Y}{2}g'_1 \pm |t'|^{1/2} \left(-\frac{3g_2}{2} + \frac{Y}{2}g'_2 \right) \pm |t'| \left(-2h + \frac{3X}{2}h_X + \frac{Y}{2}h_Y \right),$$

and

$$z_x = |t'|^{1/2}h_X, \quad z_y = \mp |t'|^{1/2}g'_1 + |t'| (g'_2 - 2BYh_X) + |t'|^{3/2}h_Y.$$

Inserting into (8) gives

$$1 - \left(g_1 - \frac{Y}{2}g'_1 \right)^2 = 0$$

to leading order, with solution $g_1 = 1 + AY^2$. At the next order $t'^{1/2}$, we have

$$2 \left(\frac{3g_2}{2} - \frac{Y}{2}g'_2 \right) = 0,$$

and so $g_2 = CY^3$. Finally, at order t' this gives the similarity equation

$$4h - 3Xh_X - Yh_Y \pm h_X^2 \pm 4A^2Y^2 = 0. \quad (29)$$

In order to see that (20)/(21) solves (29) one notes that (29) linearizes when assuming

$$\hat{X}(\zeta, Y) = X \quad \text{and}$$

$$\hat{h}(\zeta, Y) = h(\hat{X}(\zeta, Y), Y) \quad (30)$$

to satisfy

$$\hat{h}_\zeta = \epsilon \zeta^n \hat{X}_\zeta \quad (31)$$

(for the case of (20)/(21) $n = 1$ and $\epsilon = 2$). Using

$$h_X = \frac{\hat{h}_\zeta}{\hat{X}_\zeta}, \quad h_Y = \hat{h}_Y - \frac{\hat{h}_\zeta}{\hat{X}_\zeta} \hat{X}_Y, \quad (32)$$

and (31), one gets an inhomogeneous *linear* equation,

$$4\hat{h} - 3\epsilon \zeta^n \hat{X} - Y\hat{h}_Y + \epsilon \zeta^n Y \hat{X}_Y = \mp \epsilon^2 \zeta^{2n} \mp 4A^2Y^2. \quad (33)$$

The Ansatz

$$\begin{aligned} \hat{h} &= \epsilon(a-n)\zeta^a Y^b + \epsilon \gamma n \zeta^{2n} \mp 2A^2Y^2 \\ \hat{X} &= a\zeta^{a-n} Y^b + 2n\gamma \zeta^n \end{aligned} \quad (34)$$

gives

$$\gamma = \pm \frac{\epsilon}{2n}, \quad a + bn = 4n, \quad (35)$$

and due to the linearity, arbitrary linear combinations of the homogeneous (a, b) solutions can be taken (explaining the linear abundance of free constants in (20)/(21)).

Note that the quadratic terms Y^2 in (20),(21) can be understood as a shift in t' . Thus (putting all $A_{i \neq 2}$ equal to zero) one can consider the Ansatz

$$z = \mp |t'| \left(1 + AY^2 \right) + \left(|t'| + A_2Y^2 \right)^2 \tilde{h} \left(\frac{x - By^2}{(|t'| + A_2Y^2)^{3/2}} \right), \quad (36)$$

which means that

$$h(X, Y) = \left(1 + A_2Y^2 \right)^2 \tilde{h} \left(\frac{X}{(1 + A_2Y^2)^{3/2}} \right) \mp 2A^2Y^2 \quad (37)$$

in (28).

Indeed, it is easy to confirm that if \tilde{h} satisfies the one-dimensional similarity equation

$$4\tilde{h} - 3\xi \tilde{h}_\xi \pm \tilde{h}_\xi^2 = 0, \quad (38)$$

then (37) satisfies (29), which possess swallowtail-type self similar solutions of the form [4]

$$\xi = \pm \zeta + c\zeta^3/3, \quad h(\xi) = \pm \zeta^2/2 + c\zeta^4/4 \quad (39)$$

whose occurrence is manifested in our numerical results (see chapter 5).

4 Shape-equation for membranes near a singularity

While above we have seen that the singularities of relativistic M-branes are described by those of the eikonal equation, it is valuable to insert the Ansatz (28) also into the (full, second order) Born-Infeld equation (11). To do so (for $M = 2$), it turns out to be much simpler (and more insightful) to perform the transformation

$$\begin{aligned} t, x, y \rightarrow T := |t_0 - t| = |t'|, \quad X(t, x, y) = \frac{x - By^2}{|t'|^{\frac{3}{2}}}, \quad Y(t, x, y) = \frac{y}{\sqrt{|t'|}} \\ z(t, x, y) = Z(T(t), X(t, x, y), Y(t, y)), \end{aligned} \quad (40)$$

implying

$$\dot{z} = \mp \dot{Z} \pm \frac{1}{2T}(3XZ_X + YZ_Y), \quad z_x = \frac{1}{T^{\frac{3}{2}}}Z_X, \quad z_y = \frac{Z_Y}{\sqrt{T}} - \frac{2BY}{T}Z_X, \quad (41)$$

in the action-functional (cp. (1)/(11)) $\int \sqrt{1 - \dot{z}^2 + z_x^2 + z_y^2} dt dx dy$, yielding

$$\begin{aligned} S = \int dT dX dY T^2 \left(1 - \dot{Z}^2 - \frac{1}{4T^2}(3XZ_X + YZ_Y)^2 + \frac{\dot{Z}}{T}(3XZ_X + YZ_Y) + \frac{Z_X^2}{T^3} \right. \\ \left. + \frac{Z_Y^2}{T} + \frac{4B^2 Y^2}{T^2} Z_X^2 - \frac{4BYZ_X Z_Y}{T^{\frac{3}{2}}} \right)^{\frac{1}{2}}, \end{aligned} \quad (42)$$

from which the equations

$$\begin{aligned} \partial_T \left\{ \frac{T^2}{\sqrt{\dots}} \left[-\dot{Z} + \frac{1}{2T}(3XZ_X + YZ_Y) \right] \right\} \\ + \partial_X \left\{ \frac{T^2}{\sqrt{\dots}} \left[-\frac{1}{4T^2}(3XZ_X + YZ_Y)3X + \frac{3}{2T}\dot{Z}X + \frac{Z_X}{T^3} + \frac{4B^2}{T^2}Y^2 Z_X - \frac{2BYZ_Y}{T^{\frac{3}{2}}} \right] \right\} \\ + \partial_Y \left\{ \frac{T^2}{\sqrt{\dots}} \left[-\frac{1}{4T^2}(3XZ_X + YZ_Y)Y + \frac{1}{2T}\dot{Z}Y + \frac{Z_Y}{T} - \frac{2BYZ_X}{T^{\frac{3}{2}}} \right] \right\} = 0 \end{aligned} \quad (43)$$

follow.

Now using the Ansatz (cp. (28))

$$Z = \mp T(1 + AY^2) + CY^3 T^{\frac{3}{2}} + T^2 h(X, Y), \quad (44)$$

i.e. inserting

$$\begin{aligned} \dot{Z} = \mp T(1 + AY^2) + \frac{3}{2}CY^3 \sqrt{T} + 2Th(X, Y) \\ Z_X = T^2 h_X(X, Y), \quad Z_Y = \mp 2ATY + 3CY^2 T^{\frac{3}{2}} + T^2 h_Y(X, Y) \end{aligned} \quad (45)$$

into (43), it is, in this form (all numerators in (43) being *linear* w.r.t. (45) and the square-root in leading order being proportional to \sqrt{T}) extremely simple to identify the shape equation; one finds

$$\frac{\pm \frac{3}{2}}{\sqrt{\pm}} + \partial_X \left(\frac{h_X - \frac{3}{2}X}{\sqrt{\pm}} \right) \mp \frac{1}{2} \partial_Y \left(\frac{Y}{\sqrt{\pm}} \right) = 0 \quad (46)$$

where

$$\sqrt{\pm} = \sqrt{\pm(4h - 3Xh_X - Yh_Y) + (h_X^2 + 4A^2 Y^2)}. \quad (47)$$

Writing (46) in the form

$$\sqrt{\pm}^2 (h_{XX} \mp \frac{1}{2}) = \mp \frac{1}{4} Y \partial_Y (\sqrt{\pm}^2) + \frac{1}{2} (h_X \mp \frac{3}{2}X) \partial_X (\sqrt{\pm}^2) \quad (48)$$

one could claim it to be obvious that (29) provides asymptotic solutions of (11), while a more convincing argument is perhaps to note that (29) "in leading T-order" minimizes (42), hence must be a stationary point of (42).

5 Axially symmetric membranes

In the case of a closed string in the plane (4) (with $\mathbf{x} = \begin{pmatrix} r \\ z \end{pmatrix}$) simplifies to

$$r' \dot{r} + z' \dot{z} = 0 \quad (49)$$

$$\dot{r}^2 + \dot{z}^2 + \frac{(z'^2 + r'^2)}{\rho^2} = 1 \quad (50)$$

where $r = r(t, \varphi)$, $z = z(t, \varphi)$, $t > 0$, $\varphi \in (0, 2\pi)$, $\dot{r} = \frac{\partial r}{\partial t}$, $r' = \frac{\partial r}{\partial \varphi}$. By a suitable reparametrization one gets

$$r' \dot{r} + z' \dot{z} = 0 \quad (51)$$

$$\dot{r}^2 + \dot{z}^2 + \frac{(z'^2 + r'^2)}{\lambda^2} = 1 \quad (52)$$

where λ is a constant. The general solution is given by

$$\mathbf{x}' = \lambda \cos(F(\varphi, t)) \begin{pmatrix} -\sin(G(\varphi, t)) \\ \cos(G(\varphi, t)) \end{pmatrix} \quad (53)$$

$$\dot{\mathbf{x}} = -\sin(F(\varphi, t)) \begin{pmatrix} \cos(G(\varphi, t)) \\ \sin(G(\varphi, t)) \end{pmatrix} \quad (54)$$

with the integrability condition $\partial_t \mathbf{x}' = \partial_\varphi \dot{\mathbf{x}}$ solved by $G(\varphi, t) = f(\varphi + \frac{t}{\lambda}) + g(\varphi - \frac{t}{\lambda})$ and $F(\varphi, t) = f(\varphi + \frac{t}{\lambda}) - g(\varphi - \frac{t}{\lambda})$.

Closedness of the string implies that when one starts the time evolution with a regular initial data, i.e. $F(t=0, \varphi) \in (-\frac{\pi}{2}, \frac{\pi}{2})$ then F always attains the value $\frac{\pi}{2}$ in a finite time. This shows that the curvature of the string

$$k(\varphi, t) = \frac{G'}{\rho \cos(F)} \quad (55)$$

diverges there, hence singularities (as first observed in [5]) are unavoidable. Since the $M = 2$ case with rotational symmetry is very similar to the string case (a rotationally symmetric shape is described by a curve in the plane) one could try to perform a similar analysis for axially symmetric membranes, i.e. for \mathbf{x} of the form

$$\mathbf{x}(t, \varphi, \psi) = \begin{pmatrix} r(t, \varphi) \cos \psi \\ r(t, \varphi) \sin \psi \\ z(t, \varphi) \end{pmatrix} \quad (56)$$

In this case (4) becomes

$$r' \dot{r} + z' \dot{z} = 0 \quad (57)$$

$$\dot{r}^2 + \dot{z}^2 + \frac{r^2(z'^2 + r'^2)}{\rho^2} = 1 \quad (58)$$

whose general solution can be again parametrized by two functions F and G

$$\frac{r}{\rho} \mathbf{x}' = \cos(F(\varphi, t)) \begin{pmatrix} -\sin(G(\varphi, t)) \\ \cos(G(\varphi, t)) \end{pmatrix} \quad (59)$$

$$\dot{\mathbf{x}} = -\sin(F(\varphi, t)) \begin{pmatrix} \cos(G(\varphi, t)) \\ \sin(G(\varphi, t)) \end{pmatrix} \quad (60)$$

However in this case the integrability conditions remain unsolved. One can still express the curvature of the curve (giving rise to the solid of revolution) in a concise way

$$k(\varphi, t) = \frac{r}{\rho} \frac{G'}{\cos F}. \quad (61)$$

6 Numerical results

We first present, for various initial conditions, numerical solutions (obtained with Mathematica) to the evolution equations (58) rewritten in the more convenient form

$$\dot{r} = -z' \sqrt{\frac{1}{z'^2 + r'^2} - \frac{r^2}{\rho(\varphi)^2}} \quad (62)$$

$$\dot{z} = r' \sqrt{\frac{1}{z'^2 + r'^2} - \frac{r^2}{\rho(\varphi)^2}}. \quad (63)$$

We then also attack the system (4) without assuming radial symmetry. All numerical data confirm that the embedding functions are smooth.

Ellipsoid

We consider an initial shape of the form of an ellipse

$$r(0, \varphi) = a \sin(\varphi) \quad z(0, \varphi) = -\cos(\varphi)$$

with a homogeneous initial density distribution, i.e. $\dot{\mathbf{x}}^2 = v^2 = \text{const}$

$$\rho = \frac{a \sin(\varphi) \sqrt{a^2 \cos^2(\varphi) + \sin^2(\varphi)}}{\sqrt{1 - v^2}}$$

Let us first consider the case $a > 1$. The time evolution is presented in Fig 2-3. We can see that the object initially remains smooth and then develops a swallowtail (popping up first at the equator, see also the cross-section curves which grows up towards the poles and finally vanishes after some time. On the other hand, when one starts with $a < 0$ (Fig. 4) then again a swallowtail is observed, but in this case it develops first at the poles and grows up towards the equator where it disappears and the shape becomes smooth again

As one can see in Fig 3 we obtained a non-generic axial singularity of the $r \rightarrow 0$ type. It can be described by the ansatz

$$r(\varphi, t) = A(t) + B\varphi^2 \quad (64)$$

$$z(\varphi, t) = C(t)\varphi \quad (65)$$

Eq.(49) gives

$$2\dot{A}B + \dot{C}C = 0 \quad (66)$$

which integrates to (α is a constant)

$$C^2 = \alpha - 4AB \quad (67)$$

Eq. (50) at the lowest order gives

$$\dot{A}^2 = 1 \quad (68)$$

Thus $A = t - t_0$ and $C = \pm \sqrt{\alpha - 4B(t - t_0)}$. In Fig. (5) we present a comparison of this ansatz (with some choice of the constants α and B) with the numerics for an ellipsoid.

Torus

As the initial shape we take a torus

$$r(0, \varphi) = R + \cos(\varphi) \quad z(0, \varphi) = \sin(\varphi), \quad \varphi \in (0, 2\pi), R > 1$$

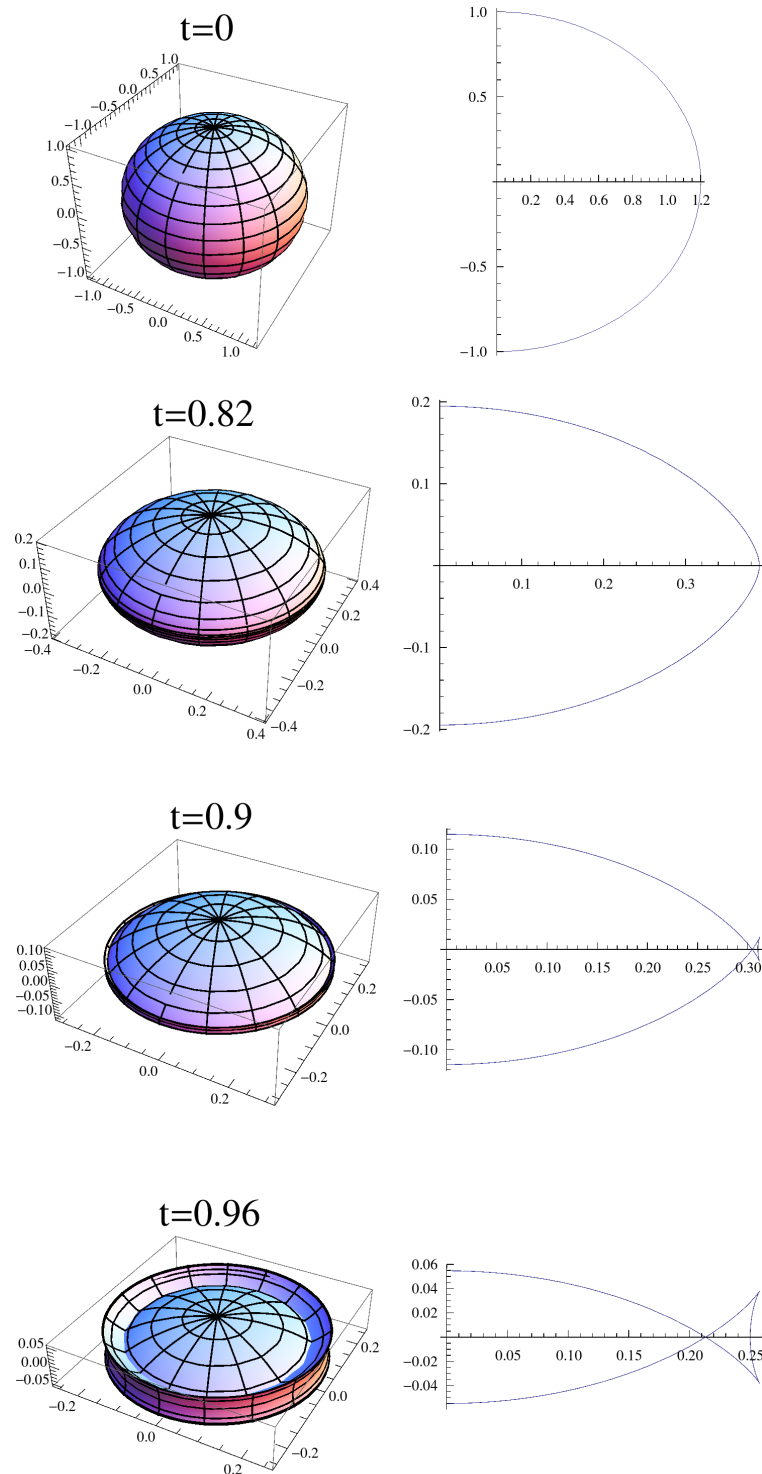


Figure 2: A typical time evolution of an ellipsoid with $a > 1$. The swallowtail first appears at the equator and then grows towards the poles. The pictures on the left show full 3-dimensional pictures while those on the right are cross sections along the rotational axis

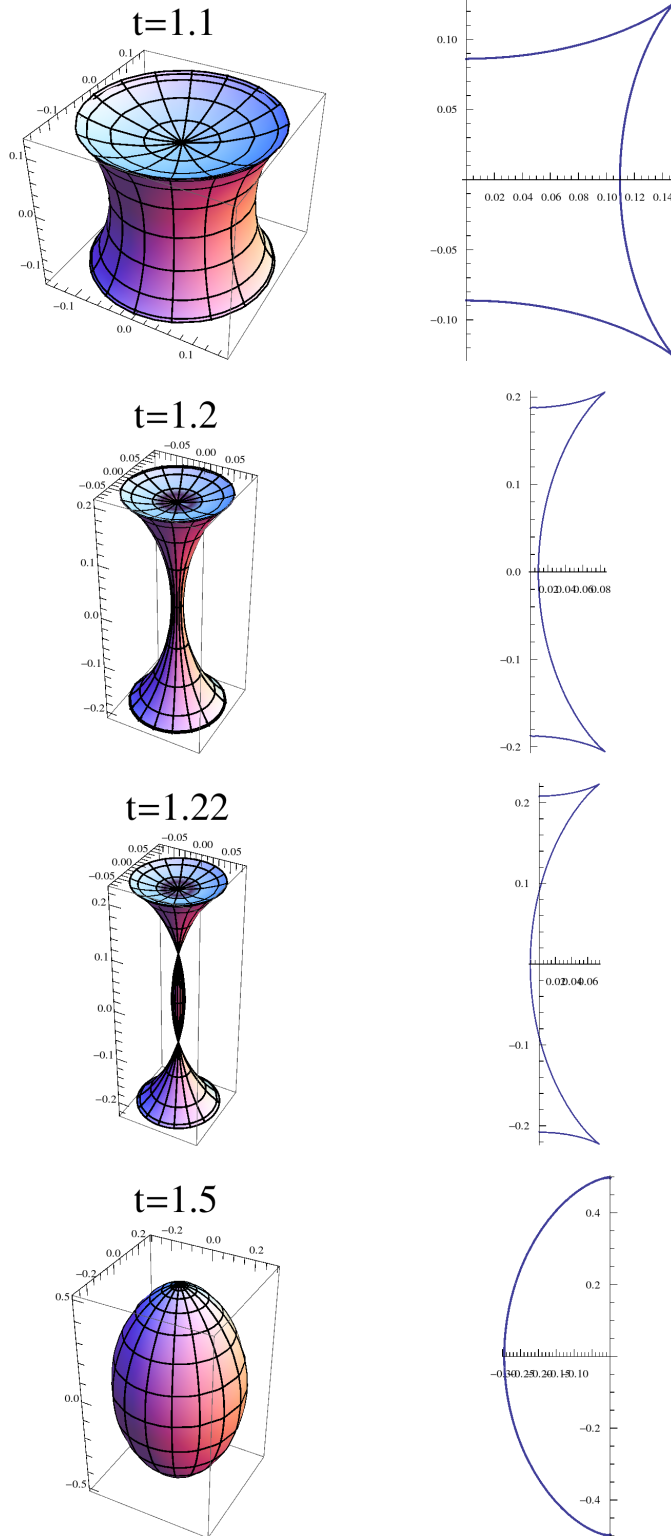


Figure 3: A typical time evolution of an ellipsoid with $a > 1$ (continuation). The swallowtail disappears at the poles and the shape becomes regular again. The pictures on the left show full 3-dimensional pictures while those on the right are cross sections along the rotational axis

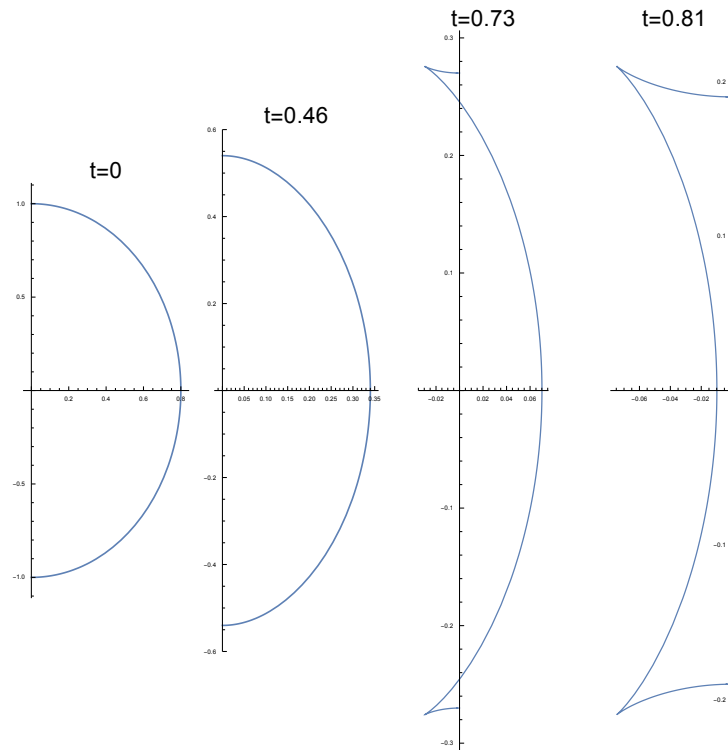


Figure 4: A typical time evolution of an ellipsoid with $a < 1$ (cross sections along the rotational axis). This time the swallowtail first appears at the poles.

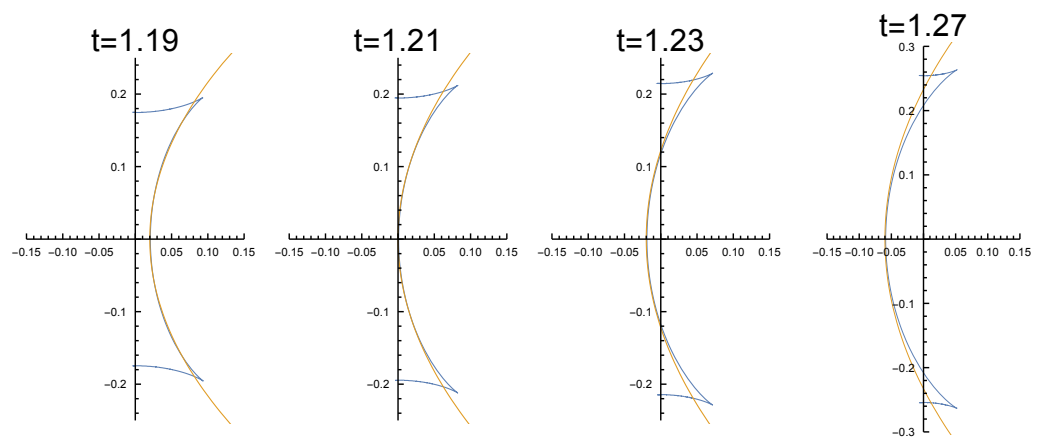


Figure 5: A comparison of the numerics and the ansatz for non-generic singularities of the $r \rightarrow 0$ type around $\varphi = 0$ for an ellipse.

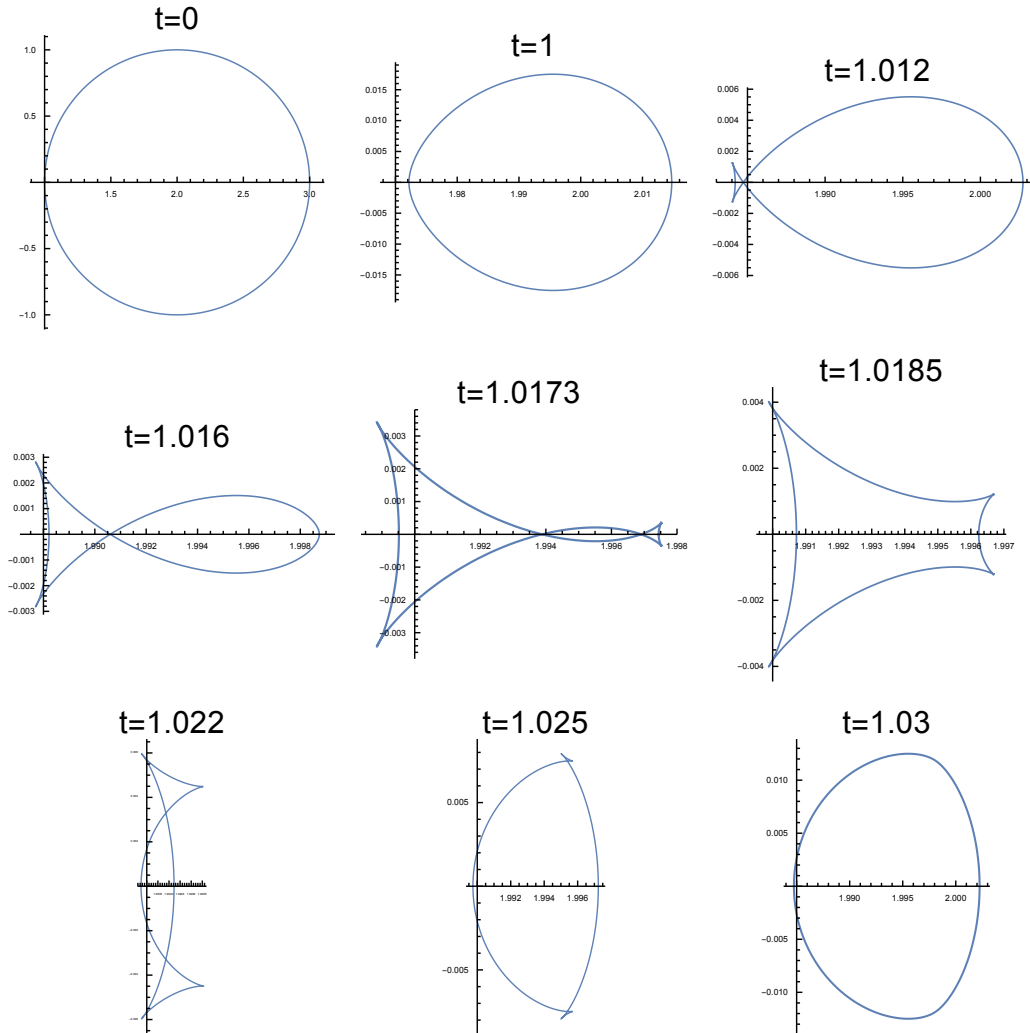


Figure 6: Time evolution (cross section along the rotational axis) of a torus. As for the ellipse, two swallowtails are being developed (however at different times). Note that the shape is drastically shrinking, i.e. the different scales in the above pictures.

with a homogeneous velocity distribution

$$\rho = \frac{R + a \cos(\varphi)}{\sqrt{1 - v^2}}$$

The time evolution presented in Fig. 7 shows that the initial shape shrinks almost to a loop and then extends back to the original shape. A closer look onto the cross-section curves around $t=100$ reveals that again a swallowtail has been developed

Elliptorus

The initial shape is a deformed torus with an ellipse as the cross-section

$$r(0, \varphi) = R + a \cos(\varphi) \quad z(0, \varphi) = \sin(\varphi), \quad \varphi \in (0, 2\pi), \quad R > a$$

density

$$\rho = \frac{R + \cos(\varphi)}{\sqrt{1 - v^2}} \sqrt{a^2 \sin^2(\varphi) + \cos^2(\varphi)}$$

We take $a > 1$ first. The time evolution is very similar to the previous case. However here we can see that the swallowtails appear simultaneously (according to the precision of the numerical solution) on both sides of

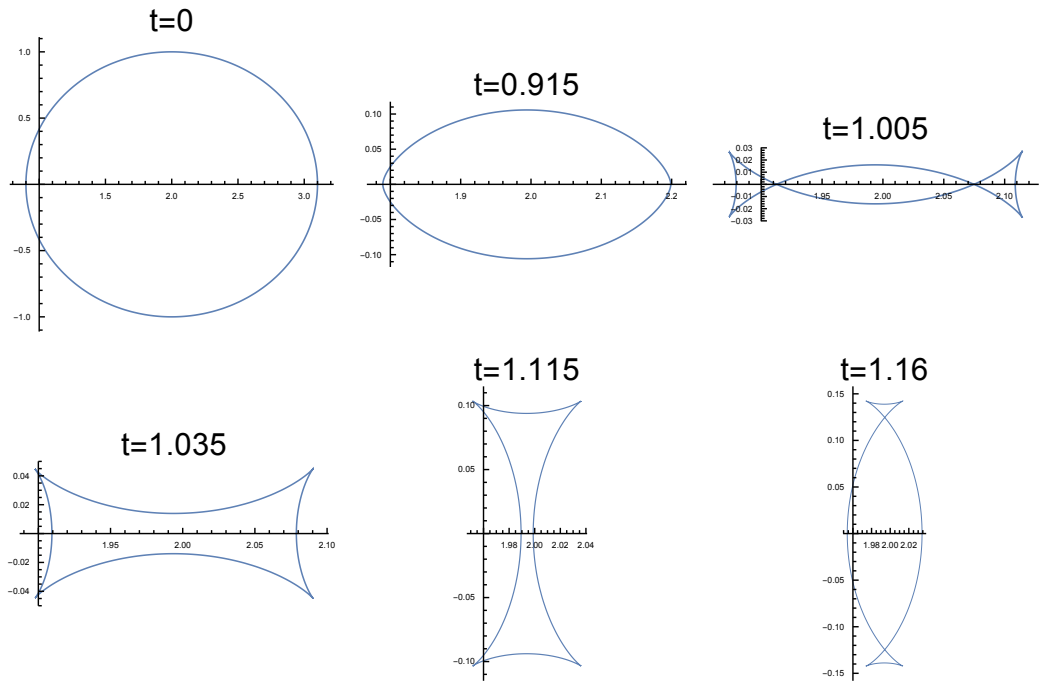


Figure 7: Time evolution (cross section along the rotational axis) of an elliptorus. This time the swallowtails are observed simultaneously.

the curve (the two points of highest initial curvature i.e. $r'^2 + z'^2$ minimal) while for the torus the swallowtail closer to the rotation axis was developed first.

General 3D case

We consider the system (4) in three space dimensions (without axial symmetry) written in a dynamical form (cp. (12))

$$\dot{\mathbf{x}} = \pm \frac{\partial_1 \mathbf{x} \times \partial_2 \mathbf{x}}{|\partial_1 \mathbf{x} \times \partial_2 \mathbf{x}|} \sqrt{1 - \frac{g}{\rho^2}} \tag{69}$$

with a uniform initial velocity distribution i.e. $\dot{\mathbf{x}}^2 = v^2 = const.$ and an ellipsoid as the initial condition,

$$\begin{aligned} x(0) &= a \cos \varphi \cos \theta \\ y(0) &= b \sin \varphi \cos \theta \\ z(0) &= c \sin \theta, \end{aligned} \tag{70}$$

with $a = 1, b = 1.2, c = 1.4$, where $\varphi \in [0, 2\pi], \theta \in [-\frac{\pi}{2}, \frac{\pi}{2}]$ and the \pm sign is chosen in such a way that the shape initially shrinks. Here we also observe swallowtails (in planar cross-sections) formed first at the points of highest initial curvature i.e. at the poles (see Fig. 8). Note that the characteristic shape of a lip is also observed (Fig. 9).

Acknowledgement: We would like to thank Pawel Biernat for e-mail correspondence, Anna-Karin Tornberg for discussions, and the Swedish Research Council, as well as NRF 2013, for support. J. Eggers and N. Suramlishvili’s work was funded by a Leverhulme Trust Research Project Grant.

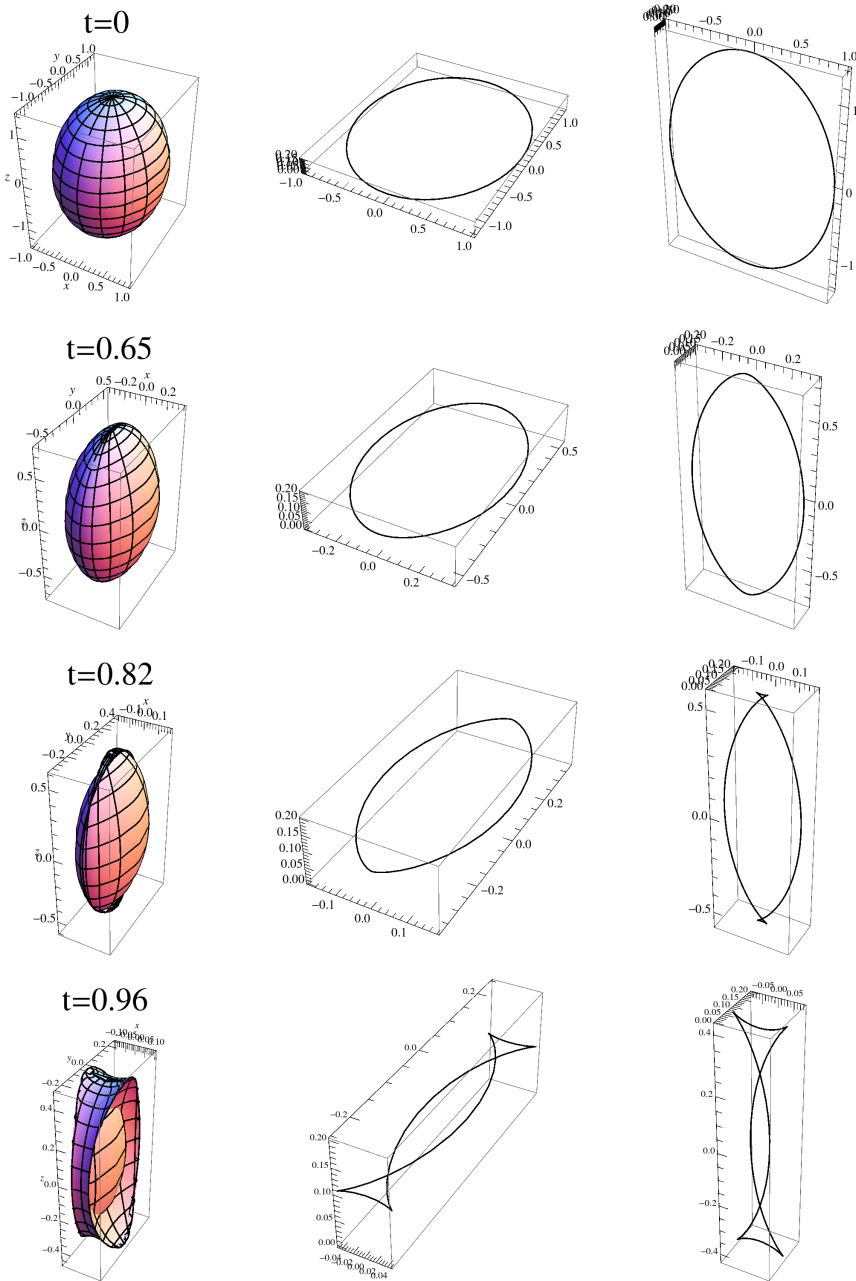


Figure 8: Time evolution of a non axially-symmetric ellipsoid with the axes of length $a = 1$, $b = 1.2$, $c = 1.4$ and a homogeneous initial velocity distribution. On the left full 3 dimensional pictures, in the middle the cross section by the $z = 0.1$ plane and on the right the cross section by the $y = 0.1$ plane. The singularity first appears at the poles. Note that at $t = 0.82$ the first cross section is still regular while the other one has already formed a swallowtail.

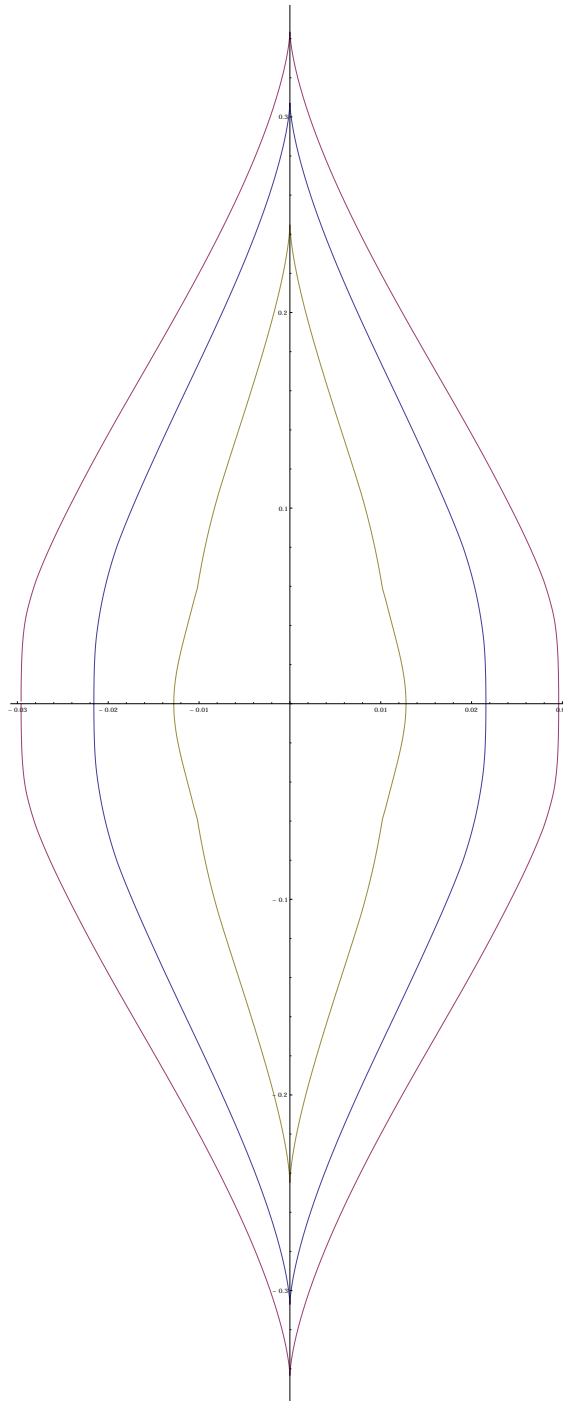


Figure 9: The places where the surface has a singularity projected onto the $x - y$ plane $t' = 0.06, 0.1$ and 0.12 after the singularity had formed. One can check that the width of the shape scales approximately like $|t'|^{\frac{3}{2}}$ and the height like $|t'|^{\frac{1}{2}}$. Here due to the reflection symmetry the lip is also symmetric (compare with Fig. 1).

References

- [1] V. I. Arnol'd, V. A. Vasil'ev, V. V. Goryunov, and O. V. Lyashko, in *Dynamical Syatems VIII* (Springer, Heidelberg, 1993).
- [2] G. Bellettini, J. Hoppe, M. Novaga, G. Orlandi, *Complex Anal. Operator Theory* **4**, 3 (2010).
- [3] J. Eggers and M.A. Fontelos, *The role of self-similarity in singularities of partial differential equations*, *Nonlinearity* **22**, R1 (2009).
- [4] J. Eggers and J. Hoppe, *Phys. Lett. B* **680**, 274 (2009).
- [5] J. Hoppe, in *Nonlinear Waves, Gakuto International Series: Mathematical Sciences and Applications, Vol. 8* (Gakkotosho, Tokyo, 1996), URL <http://arxiv:hep-th/9503069>.
- [6] J. Hoppe, *J. Phys. A: Math. Theor.* **46**, 023001 (2013).
- [7] J. Nye, *Natural Focusing and Fine Structure of Light: Caustics and Wave Dislocations* (Institute of Physics Publishing, Bristol, 1999).
- [8] L. Nguyen and G. Tian, *Class. Quantum Grav.* **30**, 16 (2013).
- [9] Y. Pomeau, M. Le Berre, P. Guyenne, and S. Grilli, *Nonlinearity* **21**, T61 (2008).
- [10] N. Turok, *Nucl. Phys B* **242**, 520 (1984).